Original Article

MOLECULAR METABOLISM

Requirement of Cavin-2 for the expression and stability of IRβ in adequate adipocyte differentiation

Yusuke Higuchi [1], Takehiro Ogata [1,2,*], Naohiko Nakanishi [1], Masahiro Nishi [1], Akira Sakamoto [1], Yumika Tsuji [1], Shinya Tomita [1], Satoaki Matoba [1]

ABSTRACT

Objective: Adipogenesis plays an essential role in maintaining energy and hormonal balance. Cavin-2, one of the caveolae-related proteins, is abundant in adipocytes, the leading site of adipogenesis. However, the details of the roles of Cavin-2 in adipogenesis remain unknown. Here, we demonstrate the requirement of Cavin-2 for the expression and stability of IRβ in adequate adipocyte differentiation.

Methods: Cavin-2 knockout (Cavin-2 KO) and wild-type (WT) mice were fed with a high-fat diet (HFD) for 8 weeks. We evaluated body weight, food intake, and several tissues. Glucose homeostasis was assessed by glucose and insulin tolerance tests. Insulin signaling in epididymal white adipose tissue (eWAT) was determined by Akt phosphorylation. In vitro study, we evaluated adipocyte differentiation, adipogenesis-related genes, and insulin signaling to clarify the relationship between Cavin-2 and adipogenesis under the manipulation of Cavin-2 expression.

Results: Caveolae structure decreased in eWAT of Cavin-2 KO mice and Cavin-2 knockdown 3T3-L1 cells. Cavin-2 enhanced the stability of insulin receptor (IR) through direct association at the plasma membrane in adipocytes, resulting in accelerated insulin/IR/Akt signaling-induced adipogenic gene expression in insulin-containing solution-stimulated 3T3-L1 adipocytes. IR-mediated Akt activation also enhanced Cavin-2 and IR expression. Cavin-2 knockout mice showed insulin resistance with dyslipidemia and pathological hypertrophic adipocytes after a HFD.

Conclusions: Cavin-2 enhances IR stability through binding IR and regulates insulin signaling, promoting adequate adipocyte differentiation. Our findings highlight the pivotal role of Cavin-2 in adipogenesis and lipid metabolism, which may help to develop novel therapies for pathological obesity and adipogenic disorders.

Keywords Cavin-2; Adipogenesis; Insulin receptor; Akt; Insulin resistance; Dyslipidemia

1. INTRODUCTION

Obesity is one of the biggest health problems, and the rate of its incidence continues to increase globally. Obesity is a risk factor for several causes of death, including heart disease, stroke, and type 2 diabetes. When energy intake exceeds its expenditure, most of the excess energy is stored in the form of lipids in the adipose tissue [1]. Increased adipose tissue mass can develop through an increase in size and number of cells. Hyperplasia of adipose tissue (adipogenesis) is generally considered healthy and adaptive for maintaining proper levels of insulin sensitizing, anti-inflammatory hormone, adiponectin, and other adipokines that modulate the metabolism [2,3]. The increase in adipocyte size (hypertrophy) in pathologic obesity causes metabolic disorders via maladaptive adipogenesis [4,5]. Pathological hypertrophic adipocytes display different biochemical properties compared to smaller adipocytes [2] and promote increased secretion of proinflammatory cytokines and decreased secretion of anti-inflammatory adipokines, leading to increased insulin resistance [6]. A pathological decrease in adipose tissue also results in metabolic disorders as a consequence of insufficient adipogenesis.

The regulation of adipogenesis is an important target in the treatment of metabolic disorders, however, adipogenesis is a complex process involving many different transcription factors and is not completely understood. C/EBPα and PPARγ are well known as critical transcription factors in both adipocyte differentiation and adipogenesis and promote the expression of target genes associated with these processes. For example, thiazolidinediones (TZDs), which are PPARγ agonists, are known to be potent insulin sensitizers for type 2 diabetes mellitus. Insulin signaling is an important pathway for increasing the expression levels of C/EBPα and PPARγ [7,8]. It has been reported that insulin receptors (IRs) are concentrated at the neck of caveolae, which are involved in insulin signaling in 3T3-L1 adipocytes [9].

Caveola is a major plasma membrane domain, which is a 50–100 nm vesicular structure near the plasma membrane or is attached [10,11]. Caveolins and cavins are endogenous membrane proteins associated

[1]Department of Cardiovascular Medicine, Graduate School of Medical Sciences, Kyoto Prefectural University of Medicine, Kyoto 602-8566, Japan [2]Department of Pathology and Cell Regulation, Graduate School of Medical Sciences, Kyoto Prefectural University of Medicine, Kyoto 602-8566, Japan

*Corresponding author. Department of Pathology and Cell Regulation and Department of Cardiovascular Medicine, Graduate School of Medical Sciences, Kyoto Prefectural University of Medicine, Kyoto 602-8566, Japan. Fax: +81 75 251 5514 E-mail: ogatat@koto.kpu-m.ac.jp (T. Ogata).

Received September 29, 2021 • Revision received November 29, 2021 • Accepted December 7, 2021 • Available online 9 December 2021

https://doi.org/10.1016/j.molmet.2021.101416

Abbreviations

C/EBPα	CCAAT/enhancer binding protein α
PPARγ	peroxisome proliferator-activated receptor γ
IR	insulin receptor
CAV 1-3	caveolin 1-3
CGL	congenital generalized lipodystrophy
Akt	protein kinase B (PKB)
ERK	extracellular signal-regulated kinase
DMI	DMEM supplemented with 10% FBS, 5 μg/mL insulin, 1 μM DEX, 0.5 mM IBMX
WT	wild-type
KO	knockout
WAT	white adipose tissue
eWAT	epididymal WAT
sWAT	subcutaneous WAT
BAT	brown adipose tissue
HFD	high-fat diet
ITT	insulin tolerance test
GTT	glucose tolerance test
LMNA	lamin A/C gene

with caveolae. Caveolin exists in three isoforms (CAV1-3) and is required for caveolar formation. Cavin that assists in the maturation of caveolae exists in four isoforms (Cavin-1/polymerase I and transcript release factor (PTRF), Cavin-2/serum deprivation response gene (SDPR), Cavin-3/sdr-related gene product that binds to c-kinase (SRBC), and Cavin-4/muscle-restricted coiled-coil protein (MURC)) [12—16]. Caveolins and cavins assist not only in the formation of caveolae structure but also in various intracellular signaling pathways. CAV1, CAV3, Cavin-1, and Cavin-3 are known to be associated with adipogenesis and adipocyte differentiation [17—20]. Mutations in these genes cause lipo- and muscular dystrophies called congenital generalized lipodystrophy (CGL). Patients with CGL are extremely hypoleptinemic, and as a result, they have low energy metabolism and metabolic complications, such as diabetes mellitus [4].

Cavin-2 is highly expressed in the adipose tissue, lung, and heart [21—23]. A recent study showed that the expression level of Cavin-2 mRNA is positively correlated with those of PPARγ and C/EBPα [24]. This suggests that Cavin-2 might play a pivotal role in the differentiation and/or maturation of adipocytes, however, the role of Cavin-2 in adipocyte differentiation and lipid metabolism remains unknown.

The purpose of the present study was to explore the function of Cavin-2 in adipocyte differentiation. Here, we demonstrate that Cavin-2 is a crucial molecule for insulin/IR/Akt signaling for proper adipogenesis and lipid metabolism. Our findings highlight the pivotal role of Cavin-2 in adipogenesis and lipid metabolism and should help in developing novel therapies for pathological obesity and adipogenic disorders.

2. MATERIALS AND METHODS

2.1. Transparent methods reagents

The rabbit polyclonal antibodies to Akt (#9272), phospho-Akt (#9271), ERK (#9102), phospho-ERK (#9101), and hemagglutinin (HA), and the horseradish peroxidase-conjugated secondary antibodies (anti-mouse-HRP, and anti-rabbit-HRP) were purchased from Cell Signaling Technology, Inc. (Danvers, MA, USA); rabbit polyclonal antibody to Cavin-2 and Cavin-3 (PRKCDBP) was purchased from ProteinTech Group, Inc. (Rosemont, IL, USA); the mouse monoclonal antibody to insulin receptor β (IRβ), rabbit polyclonal antibody to Cavin-1, and the horseradish peroxidase-conjugated monoclonal antibody to GAPDH were from Abcam PLC (Cambridge, UK). Rabbit polyclonal antibodies against caveolin-1 (N-20), and insulin receptor tyrosine kinase inhibitor (HNMPA) were purchased from Santa Cruz Biotechnology, Inc. (Dallas, TX, USA). BODIPY™ 493/503 (4,4-difluoro-1,3,5,7,8-Pentamethyl-4-Bora-3a,4a-Diaza-s-Indacene), mouse *Cavin-2*, and control small interfering RNA (siRNA) duplex oligonucleotides (Silencer® Select siRNAs), Lipofectamine® RNAiMAX reagent, and TRIzol were obtained from Thermo Fisher Scientific Inc. (Waltham, MA, USA), 3-isobutyl-1-methylxanthine (IBMX) and Duolink II Detection Kit were purchased from Sigma Chemical Co. (St. Louis, MO, USA). Dulbecco's modified Eagle's medium (DMEM), penicillin/streptomycin solution (× 100), insulin solution (human, recombinant), dexamethasone (DEX), phosphate-buffered saline (PBS), 4% paraformaldehyde (PFA), isopropyl alcohol, and LabAssay™ Triglyceride Kit were purchased from FUJIFILM Wako Pure Chemical Corporation (Tokyo, Japan). Rosiglitazone was purchased from Tokyo Chemical Industry Co., Ltd. (Tokyo, Japan). Oil Red O powder was purchased from Nacalai Tesque, Inc. (Kyoto, Japan). DAPI Fluoromount-G® was purchased from Southern Biotech (Birmingham, AL, USA). The small molecule inhibitors of Akt (Akt inhibitor) were purchased from Calbiochem (San Diego, CA, USA).

2.2. Cell culture and induction of differentiation

We used 10-15th passaged 3T3-L1 cells for in vitro experiments. 3T3-L1 cells were maintained in DMEM containing 100 U/mL penicillin and 100 mg/mL streptomycin, and supplemented with 10% (v/v) heat-inactivated fetal bovine serum at 37 °C in a 5% CO_2 atmosphere. For differentiation, cells were induced 1-day post—confluence with DMEM supplemented with 10% FBS, 5 μg/mL insulin, 1 μM DEX, 0.5 mM IBMX, 100 U/mL penicillin, and 100 μg/mL streptomycin (DMI solution) for 2 days (Figure 1A). Two days after induction, the medium was changed to DMEM and supplemented with 10% FBS and 5 μg/mL insulin [25]. In acute insulin stimulation assay, differentiated 3T3-L1 adipocytes were subjected to insulin starvation for 2 days before applying the insulin stimulation (5 μg/mL) for 30 min.

2.3. Gene silencing

Mouse *Cavin-2* and control siRNAs were transiently transfected into 3T3-L1 preadipocyte cells using the Lipofectamine® RNAiMAX reagent according to the manufacturer's instructions. The medium was changed 24 h post-transfection. Suppression of Cavin-2 was confirmed by RT-qPCR and western blot analysis (Supplementary Fig. 1C).

2.4. Gene transfer

Recombinant adenoviruses expressing HA-tagged human Cavin-2 (Ad-Cavin-2-HA) and Ad-β-galactosidase (Ad-LacZ) were described previously [26]. Twenty-four hours after seeding on a plate, the 3T3-L1 preadipocyte cells were infected with Ad-Cavin-2-HA or Ad-LacZ diluted in culture medium at a multiplicity of infection (MOI) of 30 and incubated at 37 °C for 24 h. The viral suspension was removed, and the 3T3-L1 cells were cultured in fresh medium. Overexpression of Cavin-2-HA was confirmed by western blot analysis (Supplementary Fig. 1D).

2.5. Oil red O staining

To evaluate the amount of triacylglycerol (TG) in 3T3-L1 cells, Oil Red O stock solution was prepared by dissolving Oil Red O in 60% isopropyl

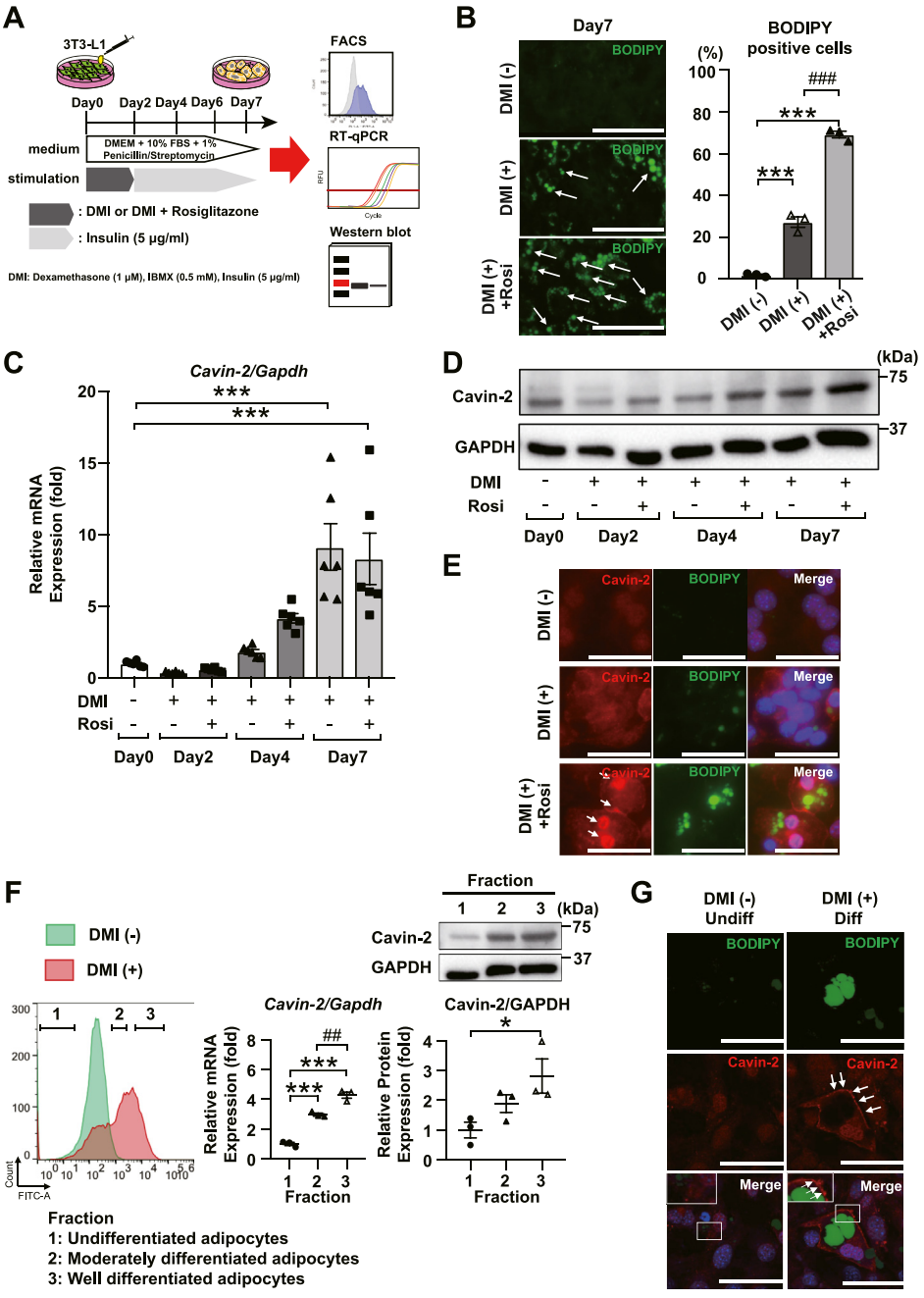

Figure 1: Cavin-2 is increased progressively at the plasma membrane during adipocyte differentiation. (**A**) Protocol of DMI-induced adipocyte differentiation in 3T3-L1 cells. **(B)** Representative fluorescent images of BODIPY-stained 3T3-L1 cells at day 7 after DMI stimulation, and flow cytometry data. White arrows indicate BODIPY-positive lipid droplets. Scale bar is 100 μm. The mRNA **(C)** and protein **(D)** expression levels of Cavin-2 in adipogenic 3T3-L1 cells. (**E**) Representative fluorescent images of BODIPY and Cavin-2 in DMI (−), DMI (+), and DMI (+) with Rosiglitazone adipocytes. Scale bar is 200 μm. White arrows indicate Cavin-2 localization at the plasma membrane in mature adipocytes. (**F**) The mRNA (center graph) and protein (right graph) expression levels of Cavin-2 in each of the adipogenic 3T3-L1 cells classified into three fractions according to the degree of adipogenesis. (**G**) Representative fluorescent images of BODIPY and Cavin-2 in undifferentiated and in well-differentiated 3T3-L1 adipocytes. Scale bar is 200 μm. White arrows indicate Cavin-2 localization at the plasma membrane in mature adipocytes. $^{*}P < 0.05$, $^{***}P < 0.001$, $^{\#\#}P < 0.01$, $^{\#\#\#}P < 0.001$. The data are shown as mean ± SEM. DMI, mixed stimulation of dexamethasone, IBMX and insulin; Rosi, rosiglitazone; Undiff, undifferentiated; Diff, differentiated.

alcohol. On day 7 after the induction of differentiation, 3T3-L1 cells were washed three times with PBS and fixed in 4% PFA for 30 min. The cells were washed with PBS and stained with Oil Red O working solution for 30 min. The cells were then washed three times with PBS and observed by microscopy.

2.6. Detection of the uptake of BODIPY-labeled fatty acid by immunofluorescence microscopy and flow cytometry

3T3-L1 preadipocytes were cultured in 12 well-plates. Seven days after the induction of differentiation, cells were stained for 20 min with BODIPY™ 493/503, which can be used as a stain for neutral lipids. We

observed the degree of lipid droplets by microscopy and evaluated the percentage of lipid droplet-positive cells with SONY SH800 cell sorter (SONY Corporation, Tokyo, Japan).

2.7. Immunofluorescence staining

3T3-L1 cells were fixed with 4% PFA at room temperature for 15 min and stained with anti-Cavin-2 (1:500), anti-HA (1:1000), anti-insulin receptor β (1:500), or BODIPY™ 493/503 (2 μM). Secondary antibodies were conjugated with Alexa Fluor 488, 555, or 647 (1:500), and the nuclei were visualized using DAPI Fluoromount-G®. Fluorescent signals were detected using a Zeiss LSM510 META Confocal Imaging System (Carl Zeiss, Jena, Germany) or a Keyence BZ-X700 digital microscope (Osaka, Japan).

2.8. Transmission electron microscopy and quantitation

3T3-L1 cells and mice eWAT of HFD for eight weeks were fixed with 2% glutaraldehyde in 0.1 M cacodylate buffer, post-fixed with 2% OsO_4, and stained with uranyl acetate and lead citrate. Microtome sections were examined under a H-7100 transmission electron microscope (HITACHI, Tokyo, Japan) and photographed at a magnification of × 80,000, × 40,000 or × 20,000. Caveolae were identified by their characteristic flask shape and location at or near the plasma membrane [27,28]. When the caveolar perimeter was measured, at least ten independent fields were quantitated for each condition.

2.9. Reverse transcription—mediated quantitative polymerase chain reaction

Quantitative reverse transcription polymerase chain reaction (RT-qPCR) was conducted as described previously [26,28]. Total RNA was extracted from cultured cells or tissues using TRIzol and reverse transcribed to cDNA using the High Capacity cDNA Reverse Transcription Kit (Applied Biosystems/Thermo Fisher Scientific, Foster City, CA, USA). The synthesized cDNA was analyzed by kinetic real-time PCR using Takara PCR Thermal Cycler Dice (Takara Bio Inc., Kusatsu, Japan) with Platinum® SYBR® Green qPCR Supermix (Invitrogen/Thermo Fisher Scientific) [16]. The primer sequences are listed in Supplementary Table 1.

2.10. Western blot analysis

Cell lysates were extracted using a lysis buffer (50 mM Tris—HCl, pH 7.5, 150 mM NaCl, 50 mM EDTA, 1% Triton X-100, and protease-phosphatase inhibitor mixture). Protein samples were subjected to SDS-PAGE and then transferred to polyvinylidene difluoride membranes that were subsequently incubated with primary antibodies against phospho-Akt, Akt, phospho-ERK1/2, ERK1/2, Caveolin-1, GAPDH, Cavin-1, insulin receptor β, IRS1, Cavin-2, and Cavin-3. Horseradish peroxidase-conjugated anti-rabbit and anti-mouse IgG (GE Healthcare, Chicago, IL, USA) were used as secondary antibodies.

2.11. Proximity ligation assay

The interaction between proteins was assessed using the Duolink II Detection Kit (Sigma—Aldrich) according to the manufacturer's specifications. The signal was visualized as a distinct fluorescent spot and was captured using a Keyence BZ-X700 digital microscope. The number of PLA signals in a cell was analyzed in each treatment group.

2.12. Immunoprecipitation

3T3-L1 cells were washed with ice-cold PBS and lysed with lysis buffer (50 mM Tris—HCl, pH 8.0, 50 mM NaCl, 1% Nonidet P-40) containing protease inhibitor cocktail (Pierce), and 60 mM octyl glucoside. Immunoprecipitation was carried out by incubating the same amount of cell lysates with magnetic beads (Magnosphere MS300/Carboxyl, COSMO BIO, Tokyo, Japan) coated with each antibody at 4 °C overnight. Beads were washed with wash buffer (50 mM Tris—HCl, pH 7.2, 50 mM NaCl, 1% Nonidet P-40) three times, and the precipitated proteins were separated by SDS—PAGE, transferred to a polyvinylidene difluoride membrane, and probed with each antibody.

2.13. Cycloheximide (CHX) chase assay

3T3L1 cells (1×10^5) were seeded in 12-well plates and incubated in a CO_2 incubator with or without DMI overnight. After 3—5 days of incubation, the medium was removed and complete medium with 10% FBS containing 100 μg/mL CHX (dissolved in DMSO) was added into each well. Cell lysates were collected at different time points (t = 0, 6, 12, 24, and 48 h) after the addition of CHX, which was followed by immunoblotting. 3T3L1 cells were infected with Ad-LacZ or Ad-Cavin-2-HA, 2 days before DMI stimulation.

2.14. Animals

Cavin-2 KO mice: Genomic *Cavin-2* DNA was isolated from R1 embryonic stem (ES) cells and used to create a *Cavin-2*-targeting construct containing *floxP* sites and the neomycin resistance gene (Supplementary Fig. 6A). The construct was generated in the pBluescript II KS + vector. The 5′-arm of homology consisted of the first *floxP* site located in the 5′-untranslated region of *Cavin-2* exon 1. The 3′-arm of homology consisted of a 2.2-kb fragment fused with the *FRT-Neo-FRT-floxP* cassette located downstream of *Cavin-2* exon 1. The targeting construct was verified by sequencing and linearized with the *Sac*II endonuclease before electroporation into R1 ES cells. Genomic DNA was extracted from G418-resistant ES cell clones. ES cell DNA was digested with *Spe*I or *Nsi*I and subjected to Southern blot analysis (Supplementary Fig. 6A). For the 5′-probe, a 478-bp fragment was PCR-amplified using mouse genomic DNA and specific *Cavin-2* primers [forward (F), 5′-AGCTTAGATGGAAATGTATTGAGAA-3′; reverse (R), 5′-GTTTAATCGTGTAAATCCAGGTACG-3′]. For the 3′-probe, a 455-bp fragment was PCR-generated using specific *Cavin-2* primers (F, 5′-TTGTATCACAGATCAATGTTTCCCTA-3′; R, 5′-ATTATTAAGAGGTCTTCC AGATAAAAA-3′). The PCR products were subsequently radiolabeled with α-[32P] deoxycytidine triphosphate by random priming (Invitrogen). DNA blots were hybridized with the radiolabeled probes and visualized by autoradiography. The wild-type (WT) allele was represented by a 5.8- or 4.8-kb band, whereas a 4.9- or a 6.5-kb band represented the correctly targeted alleles (Supplementary Fig. 6A). Five of the 300 G418-resistant ES clones that underwent homologous recombination were identified by Southern blot analysis. Two independent homologous recombinant ES clones were microinjected into blastocysts derived from C57BL/6 mice. Male chimeras were inbred with female C57BL/6 mice to generate germ line-transmitted heterozygous mice (*Cavin-2*$^{fl/+}$ mice). To induce *Cavin-2* knockout (KO) mice, *Cavin-2*$^{fl/+}$ mice were bred with those expressing the CAG promoter-driven Cre recombinase gene. The offspring were genotyped by PCR using mouse tail DNA and primers (F, 5′-AGTGCTCACTTCA-GACCAACCAG-3′; R, 5′-TCAATTCAACAAAACAGATGACTTC-3′). All aspects of animal care and experimentation performed in this study were approved by the Institutional Animal Care and Use Committee of Kyoto Prefectural University of Medicine.

2.15. GTT and ITT experiments

Cavin-2 KO or wild-type mice at the age of 12 weeks were used for the glucose tolerance test (GTT) and insulin tolerance test (ITT). The experiments were performed on 12-h fasted, conscious mice by

injecting human insulin (0.75 mU/g body weight) into the intraperitoneal cavity and measuring glucose in the tail blood immediately before and 15, 30, 60, and 120 min after injection using an Accu-Check glucometer. The area under curve (AUC) was calculated. For intravenous GTTs, mice were fasted for 6 h, anesthetized with sodium pentobarbitone, and a catheter was inserted into the left carotid artery. A bolus of glucose (2 mg/g body weight) was injected into the intraperitoneal cavity and 200 μL of blood was sampled from the carotid artery at 0, 15, 30, 60, 90, and 120 min for plasma glucose analyses. Blood was immediately centrifuged, and the plasma was frozen.

2.16. Histopathological analysis

Mice were sacrificed, and the liver and WAT were fixed with 4% PFA overnight. The fixed tissues were then embedded in paraffin. The paraffin sections were stained with hematoxylin and eosin (HE) as well as picrosirius red.

2.17. Biochemical assays of tissues

Lipids in the tissues were extracted using the Folch method [29]. Triacylglycerol concentrations were measured using the LabAssay™ Triglyceride Kit, according to the manufacturer's instructions.

2.18. Statistical analysis

The experiments were carried out at least three times, unless otherwise stated. All data are expressed as mean ± standard error. Statistical analysis was performed by one-way ANOVA followed by Tukey's post-hoc test, and *P* values below 0.05 were considered significant. Statistical analyses were performed using GraphPad Prism 8 statistical packages (GraphPad Software, Inc.).

3. RESULTS

3.1. Cavin-2 is increased progressively at the plasma membrane during adipocyte differentiation

We assessed the relationship between Cavin-2 and adipocyte differentiation (Figure 1A). Phase-contrast microscopy, Oil red O staining, and flow cytometry using BODIPY lipid probe confirmed DMI (DMEM solution containing 10% FBS, 5 μg/mL insulin, 1 μM dexamethasone [DEX], 0.5 mM 3-isobutyl-1-methylxanthine [IBMX]) stimulation-induced lipid droplet production in 3T3-L1 cells and the PPARγ agonist, rosiglitazone, promoted these processes (Figure 1B and Supplementary Figs. 1A and 1B). Cavin-2 mRNA expression was gradually increased after the initiation of adipocyte differentiation by DMI and reached a level more than 8-fold compared with that in undifferentiated 3T3-L1 cells (Figure 1C). The level of Cavin-2 progressively increased after DMI stimulation and was facilitated by rosiglitazone (Figure 1D). Immunostaining also showed that the expression of Cavin-2 was increased by rosiglitazone, especially in the nucleus and cell membrane (Figure 1E). To demonstrate that the amount of Cavin-2 correlates with the maturity of individual adipocytes, we evaluated Cavin-2 expression after classifying the degree of differentiation as low and high using flow cytometry (Figure 1F). Cavin-2 mRNA and protein expression levels increased as the degree of adipocyte differentiation progressed, being the highest in the high-differentiated group. Immunostaining showed that the expressed Cavin-2 accumulated on the plasma membrane of mature adipocytes (Figure 1G). These results suggest that one of the caveolae-related proteins, Cavin-2, plays a crucial role on the plasma membrane in adipocyte differentiation.

3.2. Cavin-2 positively regulates adipogenesis without other caveolar-related protein manipulation

To investigate the functional role of Cavin-2 in adipocyte differentiation, siRNA-mediated RNA interference was used to inhibit the translation of Cavin-2 (Supplementary Fig. 1C). DMI-induced lipid droplet production was suppressed in Cavin-2 knockdown differentiated 3T3L-L1 adipocytes (Figure 2A). Flow cytometric analysis with the BODIPY lipid probe revealed a 65% reduction in lipid accumulation in Cavin-2 knockdown differentiated 3T3-L1 adipocytes compared with that in the controls (Figure 2B). After DMI-induced adipocyte differentiation, the mRNA expression of PPARγ and C/EBPα, which are master regulators of adipogenesis, and the mRNA expression of its downstream target genes, such as FABP4 and adipokines, were significantly suppressed in Cavin-2 knockdown differentiated 3T3-L1 adipocytes compared with the respective levels in the controls (Figure 2C and Supplementary Figs. 2A and 2B). The number of caveolae in Cavin-2 knockdown differentiated 3T3-L1 adipocytes significantly decreased compared with that in the controls in electron microscopy (Figure 2D).

We evaluated the effect of Cavin-2 overexpression on adipogenesis (Supplementary Fig. 1D). Almost all 3T3-L1 cells infected by Ad-Cavin-2-HA expressed HA-tagged, and ectopic HA-tagged Cavin-2 was localized at the plasma membrane (Supplementary Fig. 1E). Cavin-2 overexpression accelerated DMI-induced lipid droplet production (Figure 2E). Flow cytometric analysis revealed an approximately 50% increase in lipid accumulation at day 7 in Cavin-2-overexpressed differentiated 3T3-L1 adipocytes compared to that in the controls (Figure 2F). Cavin-2 overexpression enhanced the mRNA expression of PPARγ, CEBPα, and their downstream target genes, the effect of which was enhanced after DMI-induced adipocyte differentiation (Figure 2G and Supplementary Figs. 3A and 3B). The size of caveolae in Cavin-2-overexpressed differentiated 3T3-L1 adipocytes significantly enlarged compared with that of the controls in electron microscopy (Figure 2H).

Since some caveolae-related proteins are involved in adipocyte differentiation, we evaluated the expression of other caveolae-related proteins by regulating the expression of Cavin-2. Western blot analysis revealed that Cavin-2 knockdown had no effect on the expression of CAV1, Cavin-1, and Cavin-3 in the undifferentiated or differentiated 3T3-L1 adipocytes (Supplementary Fig. 2C). Cavin-2 overexpression also had no effect on the expression of these caveolae-related proteins in the undifferentiated or differentiated 3T3-L1 adipocytes (Supplementary Fig. 3C). This result suggests that Cavin-2 regulates adipogenesis without affecting other caveolar-related protein manipulations.

3.3. Cavin-2 increases the expression of insulin receptor and enhances the Akt activity

We evaluated the role of Cavin-2 in IR/Akt signaling in adipogenesis because insulin receptor (IR)/Akt signaling is an important pathway to regulate protein synthesis and gene expression in adipogenesis and lipid metabolism. Akt phosphorylation was significantly increased on day 7 after adipocyte differentiation (Figure 3A). The expression level of IRβ and pAkt was significantly increased in the Cavin-2-overexpressed differentiated 3T3-L1 adipocytes than the LacZ controls, but not between the undifferentiated 3T3-L1 adipocytes (Figure 3B). Both Cavin-2 overexpression and knockdown unaffected ERK phosphorylation in the undifferentiated and differentiated 3T3-L1 adipocytes (Supplementary Figs. 2D and 3D). Immunostaining showed that the expression of IRβ was increased in the Cavin-2-

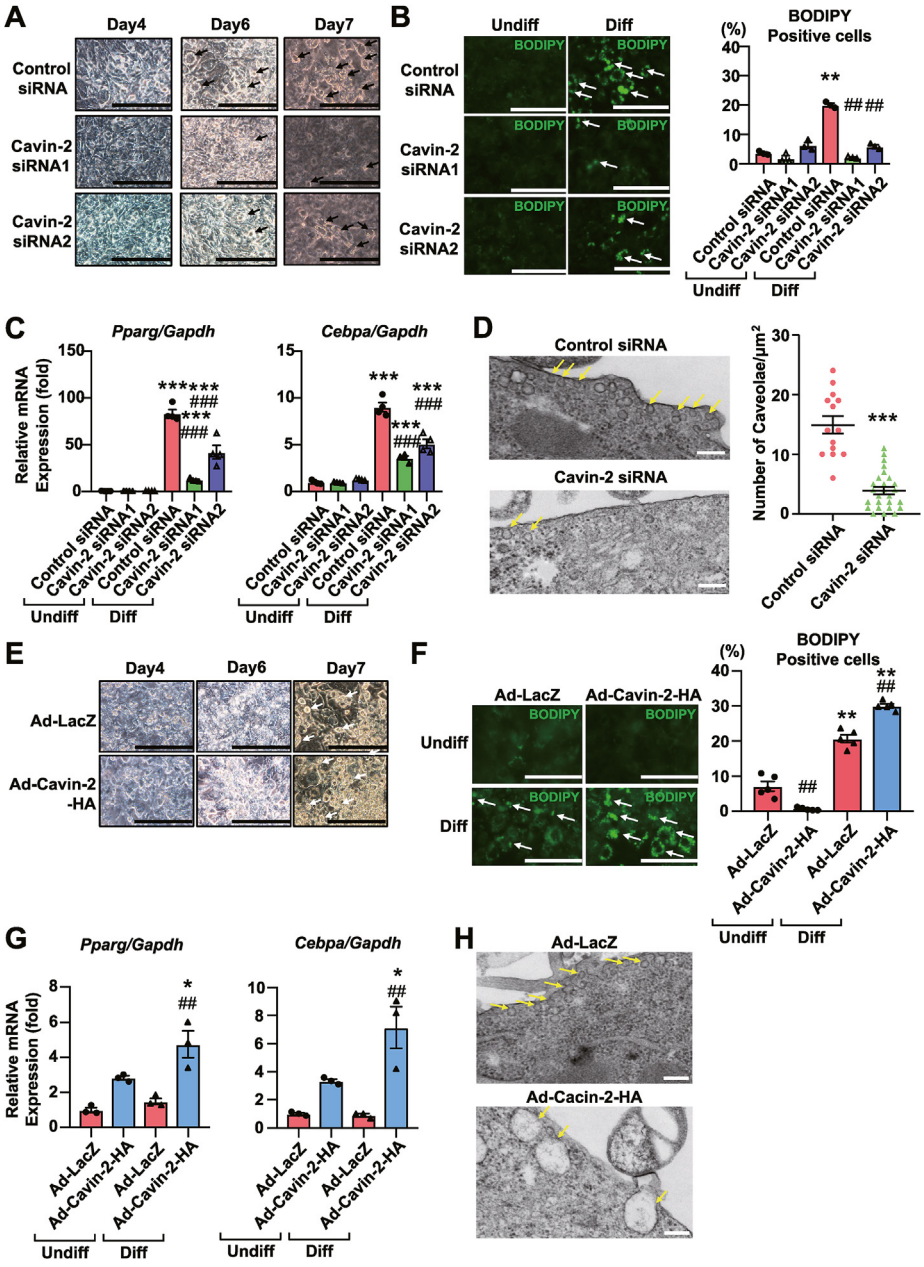

Figure 2: Cavin-2 positively regulates adipogenesis without other caveolar-related protein manipulation. (**A**) Representative phase-contrast images of Cavin-2 or control siRNA-transfected differentiated 3T3-L1 adipocytes at day 7 after DMI stimulation. Black arrows indicate lipid droplets. Scale bar is 200 μm. (**B**) Representative fluorescent images of BODIPY in 3T3-L1 cells at day 7 after DMI stimulation, and flow cytometry data. White arrows indicate BODIPY-positive lipid droplets. $^{**}P < 0.01$ vs. the respective siRNA in the undifferentiated group, $^{\#\#}P < 0.01$ vs. control siRNA in the undifferentiated or differentiated adipocyte group. Scale bar is 200 μm. (**C**) The mRNA expression levels of adipogenic genes in differentiated 3T3-L1 adipocytes at day 7 after DMI stimulation. $^{**}P < 0.01$ vs. the respective siRNA group in the undifferentiated 3T3-L1 adipocytes, $^{\#\#}P < 0.05$, $^{\#\#}P < 0.01$ vs. control siRNA in the undifferentiated or differentiated group. (**D**) Representative electron microscopic images to show the morphology of caveolae in control and Cavin-2 siRNA-transfected differentiated 3T3-L1 adipocytes. Caveolae were identified by their characteristic flask shapes and locations at or near the plasma membrane. Yellow arrows indicate caveolae of 3T3-L1 cells. Scale bar is 200 nm. The number of fields using for the measurement of the caveolar density was 14 and 26 in control siRNA group and Cavin-2 siRNA group, respectively. $^{***}P < 0.001$ vs. control siRNA-transfected cells. The data are shown as mean ± SEM. (**E**) Representative phase-contrast images of Ad-LacZ or Ad-Cavin-2-HA-infected differentiated 3T3-L1 adipocytes at day 7 after DMI stimulation. White arrows indicate lipid droplets. Scale bar is 200 μm. (**F**) Representative fluorescent images of BODIPY in adenovirus-infected differentiated 3T3-L1 adipocytes at day 7 after DMI stimulation, and flow cytometry data. White arrows indicate BODIPY-positive lipid droplets. Scale bar is 200 μm $^{**}P < 0.01$ vs. the respective adenovirus group in the undifferentiated 3T3-L1 adipocytes, $^{\#\#}P < 0.01$ vs. Ad-LacZ in the undifferentiated or differentiated group. (**G**) The mRNA expression levels of adipogenic genes in adenovirus-infected differentiated 3T3-L1 adipocytes at day 7 after DMI stimulation. $^{**}P < 0.01$, $^{***}P < 0.001$ vs. the respective adenovirus group in the undifferentiated 3T3-L1 adipocytes, $^{\#}P < 0.05$, $^{\#\#}P < 0.01$ vs. Ad-LacZ in the undifferentiated or differentiated group. The data are shown as means ± SEM. (**H**) Representative electron microscopic images of the morphology of caveolae in Ad-LacZ or Ad-Cavin-2-HA-infected differentiated 3T3-L1 adipocytes. Scale bars are 200 nm.

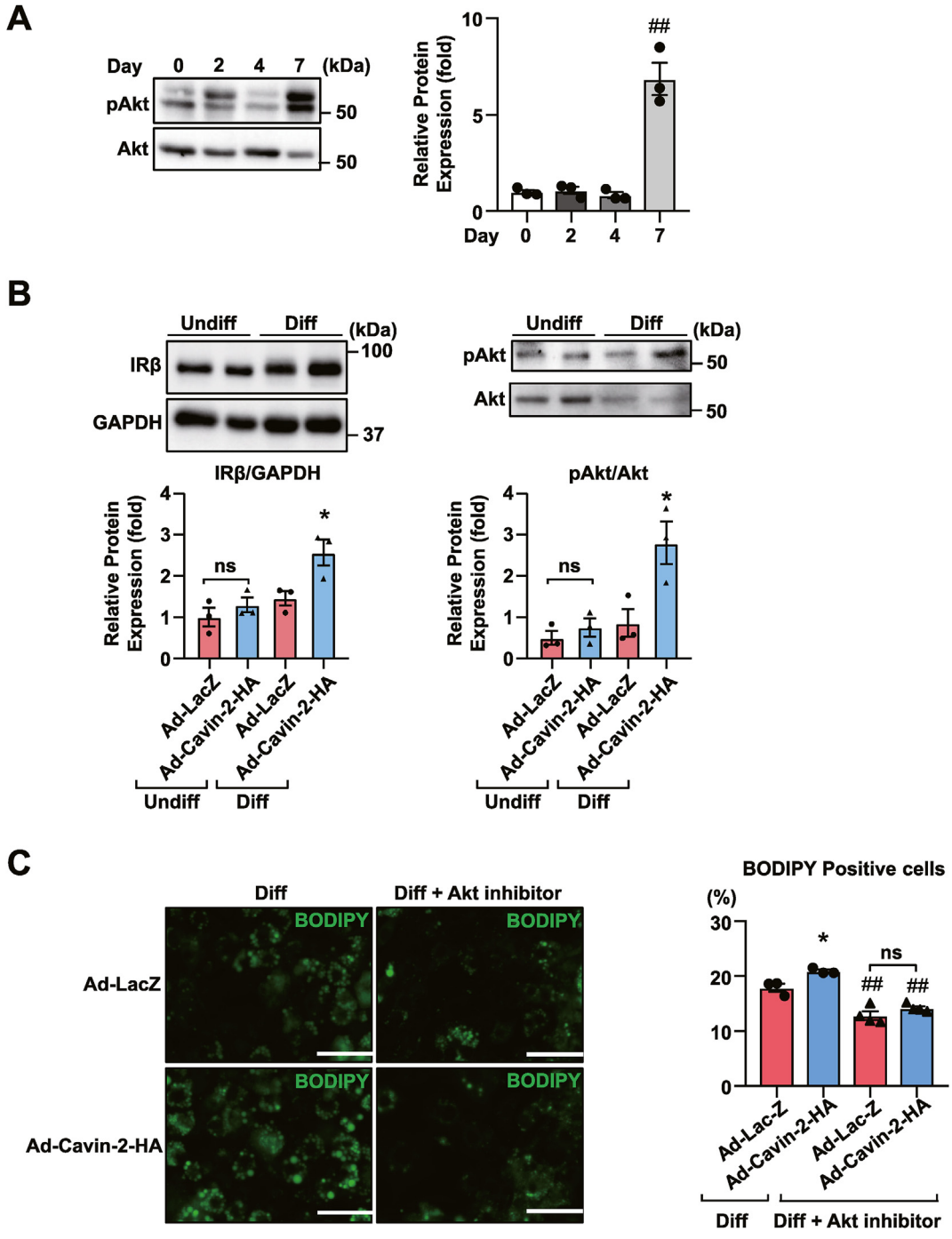

Figure 3: Cavin-2 overexpression increases the expression of insulin receptor and enhances the Akt activity. (**A**) Representative images and the quantitative data of Akt phosphorylation in adipogenic 3T3-L1 cells after DMI-induced adipocyte differentiation. (**B**) Representative western blot images and the quantitative data of IRβ and the phosphorylation of Akt in Ad-LacZ and Ad-Cavin-2-HA-infected 3T3-L1 adipocytes. $^{*}P < 0.05$ vs. Ad-LacZ. (**C**) Representative fluorescent images of BODIPY in differentiated 3T3-L1 adipocytes at day 7 after DMI stimulation (left panel), and flow cytometry data (right graph). Scale bar is 100 μm, $^{*}P < 0.05$ vs. Ad-LacZ under the same condition, $^{*}P < 0.05$ vs. Ad-LacZ. $^{\#\#}P < 0.01$ vs. the respective adenovirus-infected differentiated group without Akt inhibitor. The data are shown as mean ± SEM. ns, not significant.

overexpressed differentiated 3T3-L1 adipocytes compared with that of the LacZ controls (Supplementary Fig. 4A). The overexpression of Cavin-2 strongly promoted the expression of *Insr* mRNA (Supplementary Fig. 4B). On the contrary, the expression of IRβ was suppressed in the Cavin-2 knockdown differentiated 3T3-L1 adipocytes compared with that in the controls (Supplementary Fig. 4C). Cavin-2 knockdown also attenuated the expression of *Insr* mRNA (Supplementary Fig. 4D). The Akt inhibitor inhibited the production of lipid droplets in the Cavin-2-overexpressed differentiated 3T3-L1 adipocytes (Figure 3C and Supplementary Fig. 5). These results suggest that Cavin-2 enhances the Akt activity by increasing the expression of IRβ, resulting in the promotion of adipogenesis.

3.4. Cavin-2 interacts with IRs and enhances its stabilization at the plasma membrane

To evaluate the association with Cavin-2 and IRβ, a proximity ligation assay (PLA) was performed because Cavin-2 and IRβ are expressed at the plasma membrane during adipogenesis. PLA revealed a significant association between Cavin-2 and IRβ in the differentiated 3T3-L1 adipocytes (Figure 4A). The results of immunoprecipitation showed that Cavin-2 was associated with IRβ in the differentiated 3T3-L1 adipocytes (Figure 4B). The interaction between Cavin-2 and IRβ was increased in the Cavin-2-overexpressed differentiated 3T3-L1 adipocytes (Figure 4C). We verified the contribution of Cavin-2 to the stability of IRβ using a CHX assay. The stability of IRβ was significantly increased after adipocyte differentiation (Figure 4D) and by Cavin-2 overexpression (Figure 4E). Previous reports have

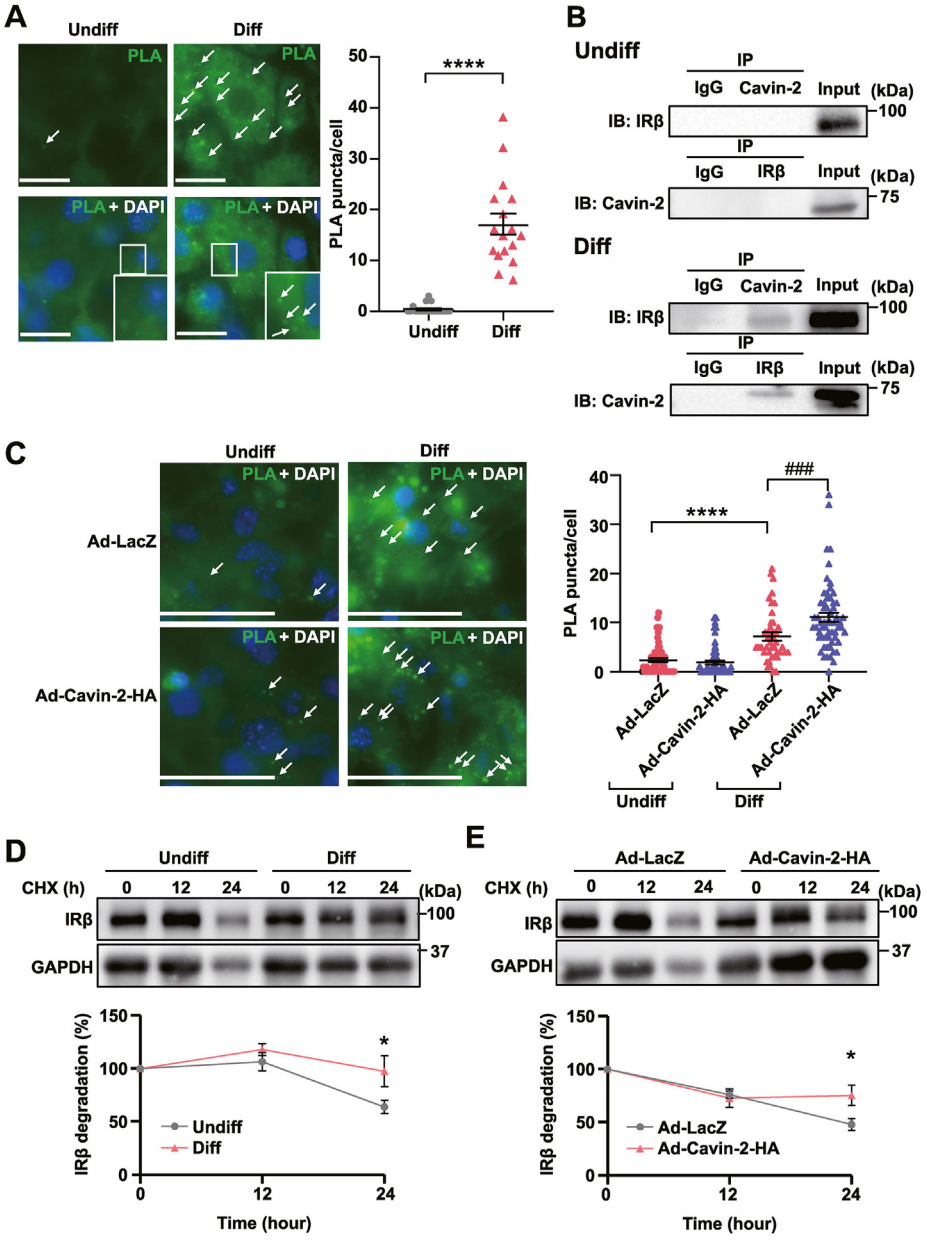

Figure 4: Cavin-2 interacts with IRβ and enhances its stabilization at the plasma membrane. (**A**) Representative fluorescent images of proximity ligation assay (PLA) for the interaction between IRβ and Cavin-2 and the quantitative data of PLA-positive signals in undifferentiated or differentiated 3T3-L1 adipocytes. White arrows indicate positive signals of IRβ-Cavin-2 interaction in the differentiated 3T3-L1 adipocytes. Scale bar is 25 μm ****$P < 0.0001$. The number of cell samples is 20 and 17 in undifferentiated and differentiated groups, respectively. (**B**) Images of coimmunoprecipitation of IRβ and Cavin-2 in undifferentiated or differentiated 3T3-L1 adipocytes. Cell lysates were coimmunoprecipitated with anti-IRβ and anti-Cavin-2 antibodies. (**C**) Representative fluorescent images of PLA for the interaction between IRβ and Cavin-2 in adenovirus-infected undifferentiated or differentiated 3T3-L1 adipocytes. The interaction between Cavin-2 and IR was enhanced in Cavin-2-overexpressed differentiated 3T3-L1 adipocytes. White arrows indicate positive signals of the IRβ-Cavin-2 interaction. Scale bar is 50 μm. The number of cell samples is 56, 55, 42, and 59 in Ad-LacZ-undifferentiated, Ad-Cavin-2-HA-undifferentiated, Ad-LacZ-differentiated, and Ad-Cavin-2-HA-differentiated, respectively. (**D, E**) Representative western blot images and quantitative data from a cycloheximide degradation assay. The data shown are the percentages of IRβ amounts relative to GAPDH. The data are shown as mean ± SEM. IR, insulin receptor; CHX, cycloheximide.

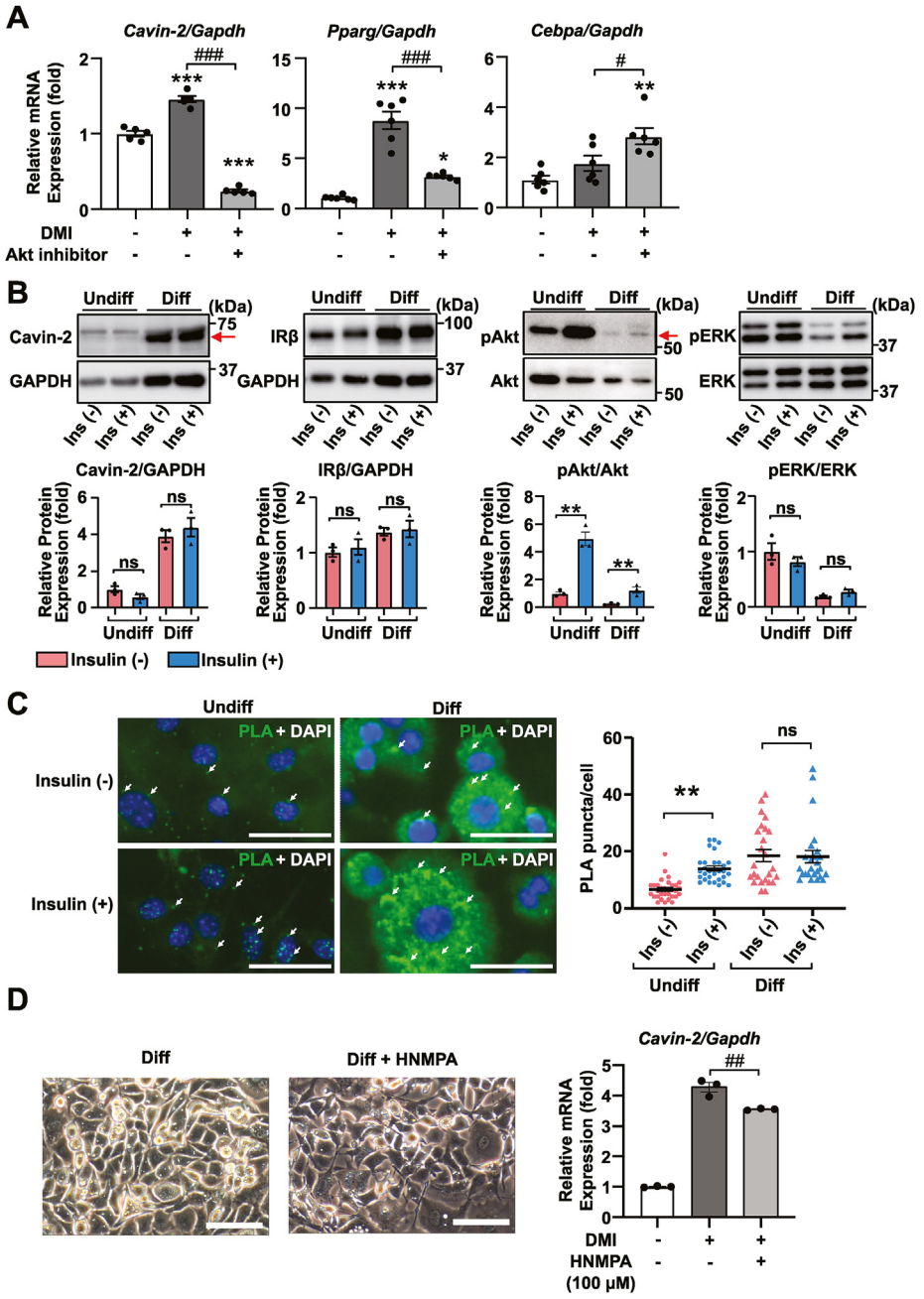

Figure 5: Cavin-2, PPARγ, and C/EBPα are downstream target genes of the IR/Akt signaling pathway. (**A**) The mRNA expression levels of Cavin-2, Pparg, and Cebpa in undifferentiated and differentiated 3T3-L1 adipocytes after the Akt inhibitor. $^{*}P < 0.05$, $^{**}P < 0.01$, $^{***}P < 0.001$ vs. the undifferentiated 3T3-L1 adipocytes, $^{\#}P < 0.05$, $^{\#\#\#}P < 0.001$. (**B**) Representative western blot images and the quantitative data of Cavin-2, IRβ, and the phosphorylation of Akt and ERK in untreated or acute insulin-treated undifferentiated and differentiated 3T3-L1 adipocytes. $^{**}P < 0.01$. (**C**) Representative fluorescent images of the PLA for the interaction between IRβ and Cavin-2 in untreated or acute insulin-treated undifferentiated and differentiated 3T3-L1 adipocytes. White arrows indicate positive signals of the IRβ-Cavin-2 interaction. Scale bar is 50 μm. The number of cell samples is 30, 30, 25, and 25 in Insulin (−)-undifferentiated, Insulin (+)-undifferentiated, Insulin (−)-differentiated, and Insulin (+)-differentiated, respectively. $^{**}P < 0.01$. (**D**) Representative phase-contrast images and the mRNA expression level of Cavin-2 in differentiated 3T3-L1 adipocytes after 100 μM HNMPA incubation. Scale bar is 100 μm $^{\#\#}P < 0.01$. The data are shown as mean ± SEM.

suggested an interaction between CAV1 and Cavin-2 [30,31]. We evaluated the interaction of IRβ with CAV1 and Cavin-1 in 3T3-L1 adipocytes. Both CAV1 and Cavin-1 showed interactions with IRβ in undifferentiated and differentiated 3T3-L1 adipocytes. There was no apparent change in the interactions with or without the Cavin-2 knockdown (Supplementary Fig. 6A).

3.5. Cavin-2, PPARγ and C/EBPα are downstream target genes of the IR/Akt signaling pathway

A recent study showed that the expression of CEBPα and PPARγ activity promote the transcription of Cavin-2 during adipogenesis [24]. To demonstrate that IR/Akt signaling is involved in the transcription of Cavin-2, we investigated the effect of an Akt inhibitor on

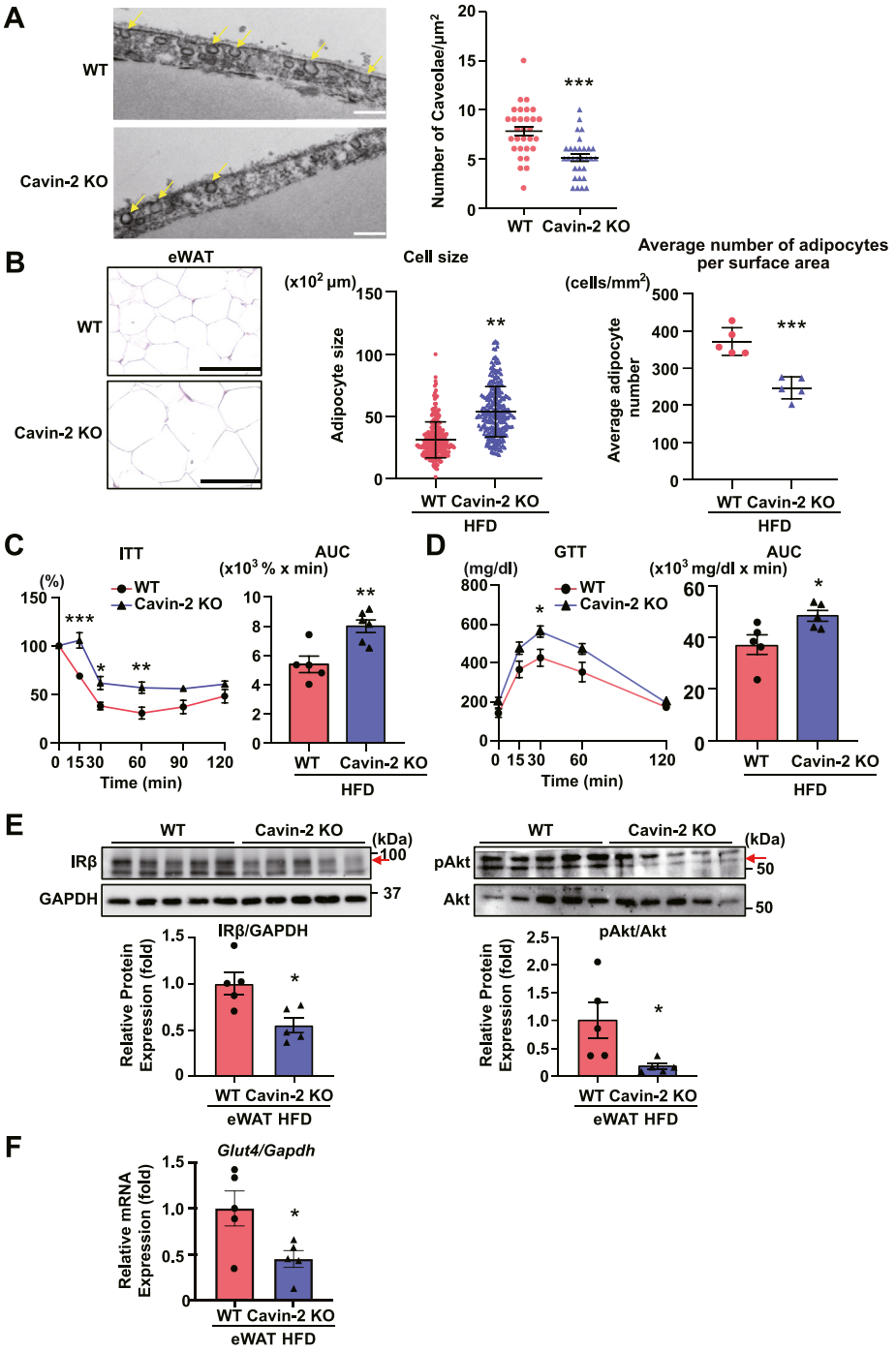

Figure 6: Cavin-2 knockout mice fed a high-fat diet show insulin resistance and dyslipidemia with an ectopic fat accumulation. (**A**) Representative electron microscopic images to show the morphology of caveolae of adipocytes in the epididymal white adipose tissues (eWAT) of the WT or Cavin-2 KO mice. Yellow arrows indicate caveolae of adipocytes. Scale bar is 200 nm. The number of fields used for the measurement of the caveolar density was 30 in each group. $^{***}P < 0.001$ vs. WT mice. The data are shown as means ± sem. (**B**) Representative images of hematoxylin-and-eosin-staining against eWAT of the WT and Cavin-2 KO mice fed the high-fat diet (HFD) for 8 weeks (left panels) and the quantitative data of the cell size of adipocytes (middle graph) or the number of adipocytes per unit area (right graph) in each mice group. The number of cell samples is 260, respectively. $^{***}P < 0.001$, $^{**}P < 0.01$ vs. WT mice. The data are shown as mean ± SEM. Insulin tolerance tests of mice fed the HFD for 3 weeks (n = 5 per group) (**C**), and glucose tolerance tests of mice fed the HFD for 4 weeks (n = 5 per group) (**D**). Each left graph shows the quantitative data of the area under the curves. $^{**}P < 0.01$, $^{*}P < 0.05$ vs. WT mice. The data are shown as mean ± SEM. Representative western blot images, quantitative data of IRβ and phosphorylation of Akt (**E**) and mRNA expression of Glut4 (**F**) in the eWAT of the WT and Cavin-2 KO mice fed with the HFD for 8 weeks (n = 5 per group). $^{*}P < 0.05$ vs. WT mice. The data are shown as mean ± SEM. GTT, glucose tolerance test; ITT, insulin tolerance test; AUC, area under the curve.

its transcription. The Akt inhibitor strongly suppressed DMI-induced expression of Cavin-2 and Pparg mRNAs. In contrast, the expression of Cebpa mRNA was significantly increased by Akt inhibition (Figure 5A).

3.6. Acute insulin stimulation stabilizes IRs and promotes insulin signaling in undifferentiated 3T3-L1 cells

Acute insulin stimulation is an important factor in adipocyte differentiation. We evaluated the effect of acute 5 μg/mL insulin stimulation on insulin-Akt signaling and the interaction between Cavin-2 and IR in the undifferentiated and differentiated 3T3-L1 adipocytes (Figure 5B). Differentiated 3T3-L1 adipocytes were evaluated by insulin starvation for 2 days and then acute 5 μg/mL insulin stimulation. The protein expression level of Cavin-2 and IRβ in the undifferentiated and differentiated 3T3-L1 adipocytes was unchanged by acute insulin stimulation regardless of adipocyte differentiation. Akt phosphorylation in the undifferentiated and differentiated 3T3-L1 adipocytes was enhanced 30 min after acute insulin stimulation. ERK phosphorylation had no response to acute insulin stimulation. We evaluated the interaction between Cavin-2 and the IR in the PLA at the same time; acute insulin stimulation significantly increased the interaction between Cavin-2 and IR in the undifferentiated 3T3-L1 adipocytes (Figure 5C). 100 μM HNMPA, a selective IR inhibitor, reduced *Cavin-2* mRNA expression in differentiated 3T3-L1 adipocytes (Figure 5D). Cavin-2 knockdown suppressed the mRNA level of GLUT4 in differentiated 3T3-L1 adipocytes (Supplementary Fig. 6B). These results indicate that acute insulin stimulation promotes insulin-Akt signaling through increasing the association between Cavin-2 and IRβ in preadipocytes.

3.7. Cavin-2 knockout mice fed a high-fat diet show insulin resistance and dyslipidemia with ectopic fatty accumulation

To assess the effect of Cavin-2-induced adipogenesis on insulin resistance, we fed a high-fat diet (HFD) to WT or Cavin-2 knockout (KO) mice for 8 weeks (Supplementary Fig. 7A). Food intake and the body weights of the two groups were comparable during the feeding of HFD (Supplementary Figs. 7B and 7C). Histological analysis revealed that the number of caveolae was significantly decreased in Cavin-2 KO mice compared to WT mice (Figure 6A). The size of adipocytes in epididymal white adipose tissue (eWAT) was larger in the Cavin-2 KO mice than in the WT mice (Figure 6B). The adipocyte number per unit area in eWATs was also decreased in Cavin-2 KO mice fed with the HFD. On the normal chow diet (NCD), the adipocyte size of eWAT in Cavin-2 KO mice was slightly larger than that in WT mice, while that of subcutaneous white adipose tissue (sWAT) was comparable between the WT and Cavin-2 KO mice (Supplementary Fig. 7D). The weights of sWAT and eWAT were comparable in the WT and Cavin-2 KO mice after the feeding of the NCD and HFD (Supplementary Fig. 7E). Total cholesterol level in Cavin-2 KO mice was higher than that in WT mice (Supplementary Fig. 7F). There were comparable blood levels of free fatty acid and triglyceride between WT and Cavin-2 KO mice (Supplementary Fig. 7F). The expression levels of Cavin-1 and CAV1 in eWAT were not different between WT and Cavin-2 KO mice fed with NCD. (Supplementary Fig. 7G). As determined by insulin tolerance test (ITT), obesity-associated insulin resistance was significantly increased in Cavin-2 KO mice (Figure 6C). Glucose tolerance test (GTT) revealed that Cavin-2 KO mice exhibited impaired glucose clearance (Figure 6D). We investigated the triglyceride concentrations in the liver to evaluate the ectopic accumulation of fat. The triglyceride concentration in the liver was significantly higher in Cavin-2 KO mice than in WT mice (Supplementary Figs. 7H and 7I). The IRβ protein expression level and the phosphorylation of Akt, not ERK, in eWAT were significantly decreased in Cavin-2 KO mice (Figure 6E and Supplementary Fig. 7J). Like IRβ expression and Akt phosphorylation, *Glut4* mRNA expression level was decreased in the eWAT of the Cavin-2 KO mice fed with the HFD (Figure 6F). Brown adipose tissue (BAT) weights were comparable after the feeding of HFD. *Ucp*-1 mRNA expression level in BATs tended to be decreased in Cavin-2 KO mice compared to WT mice (Supplementary Fig. 7K).

4. DISCUSSION

This is the first study to demonstrate the crucial molecular function of Cavin-2 in adipogenesis. Cavin-2 is abundant in adipocytes, but its functional role in these cells is not well understood. This study revealed that Cavin-2 enhanced IR stability through direct association at the plasma membrane, resulting in accelerated insulin/IR/Akt signaling-induced adipogenic gene expression. We also found that *Cavin-2* and *IRβ* are downstream targets of the IR/Akt signaling. Cavin-2 KO mice showed insulin resistance with dyslipidemia and pathologically hypertrophic adipocytes. Our findings indicate that Cavin-2 contributes to IR/Akt signaling by enhancing the stability of IR and the transcription of IR and Cavin-2 itself. Cavin-2 plays a crucial role in promoting adipogenesis and lipid metabolism.

Adipogenesis, a critical process for regulating lipid homeostasis and energy balance, is regulated by a precise cascade involving many transcription factors, such as PPARγ and the C/EBP family. Little is known about the relationship between Cavin-2 and lipogenesis. In a previous study, significant positive correlations between PPARγ, C/EBPα, and Cavin-2 were demonstrated in human subcutaneous adipose tissue and a CEBPα-dependent increase in Cavin-2 expression was observed in adipocytes [24]. In contrast, we show that Cavin-2 positively regulates adipogenesis by upregulating PPARγ and C/EBPα. At first glance, the results are contradictory, but consolidation of previous and our results suggests the existence of an unexplained feedback loop in adipogenesis.

Adipogenesis via insulin/IR/Akt signaling depends on three consecutive positive feedback loops: the first loop is between C/EBPα and PPARγ, the second is between PPARγ and C/EBPβ, and the third positive feedback loop is between PPARγ and IR [32]. Three consecutive positive feedbacks drive preadipocyte-to-adipocyte differentiation. The first loop between C/EBPα and PPARγ is essential to induce a terminally differentiated state [33–35]. Committed adipogenesis is accomplished by the addition of the second and third positive feedback loops [32]. Although the mechanism underlying the formation of these two positive feedback loops is unclear, our results suggest that Cavin-2 promotes the stabilization of IR by binding to it on caveolae, resulting in increased efficiency of insulin/IR/Akt signaling in adipogenesis. IR/Akt signaling promoted the expression of Cavin-2, suggesting that Cavin-2 is involved in both the upregulation and stabilization of IR. Our results suggest that Cavin-2 may be an important molecule in the formation of the third positive feedback loop.

The mechanism of stabilization of IR by Cavin-2 requires consideration of the effect of CAV1, which contains a scaffold domain that binds to the CAV1 binding motif in the kinase domain of IR and enhances the stability of IR [31], and play both inhibitory and stimulatory roles in insulin signaling, depending on the cellular context [30]. Our results showed that Cavin-2 did not affect the expression level of CAV1 in the differentiated 3T3-L1 adipocytes. Still, because CAV1 forms a complex with Cavin-2, the mechanism of IR stabilization and regulation of insulin signaling may involve the interaction of Cavin-2 and CAV1. Overexpression of Cavin-2 led to the enlargement of caveolae

structures. Although the size of caveolae was larger than in a previous report [36], these components were confirmed to maintain the characteristic flask shape of caveolae and opening to the extracellular space. On the other hand, in the adipocytes of Cavin-2 KO mice, the size of caveolae did not change significantly, but its density decreased. Changes in the shape and density of caveolae due to Cavin-2 can also affect the amount and density of IRs. Further studies are needed on the interaction between Cavin-2 and CAV1 as well as the relationship between caveolar structure and IR stability.

Insulin/IR/Akt signaling is an important pathway for regulating protein synthesis and gene expression in adipogenesis and lipid metabolism [37]. We demonstrate that Cavin-2 is actively involved in insulin/IR/Akt signaling in adipogenesis. A previous study reported that adipogenesis is much more strongly correlated with the Akt activity than with the PPARγ expression [32]. Akt knockout mice show severe defects in adipogenesis [38,39]. Conversely, constitutively active Akt enhances adipocyte differentiation and glucose uptake in 3T3-L1 cells [40]. Akt activation inhibits downstream substrates, such as GSK3β and Foxo1, which inhibit PPARγ and C/EBPα [41], resulting in acceleration of the transcription of PPARγ and C/EBPα. We demonstrate that the overexpression of Cavin-2 accelerated insulin-containing solution (DMI)-induced Akt phosphorylation, resulting in the promotion of adipogenesis. These effects were attenuated by the Akt inhibitor. In contrast, Cavin-2 knockdown significantly suppressed DMI-induced adipogenesis. Cavin-2 knockdown reduced the expression of PPARγ and C/EBPα mRNAs. Although the role of Cavin-2 in fat differentiation obtained in this study has not been confirmed using embryonic adipocytes, our results indicate that Cavin-2 is a strong inducer of adipogenesis and positively regulates insulin/IR/Akt-induced adipogenesis.

Cavin-2 appeared in the nuclear region in the presence of rosiglitazone. It is not clear why Cavin-2 appears in the nuclear region. Cavins are strongly involved in the caveola, and it is thought that its role is mainly played at caveolae, but a study using 3T3-L1 adipocytes has shown that Cavin-1, a member of the same cavin family as Cavin-2, is associated with the polymerase I transcription complex and has a direct role in metabolically regulated ribosomal DNA transcription [42]. Cavin-2 may play a similar role in adipose differentiation. This phenomenon may be a drug-specific response, as no nuclear translocation was observed in adipogenesis without rosiglitazone. The nuclear translocation of Cavin-2 and its role in adipogenesis is of great interest and needs to be elucidated in future studies.

To date, there is no evidence that Cavin-2 affects glucose tolerance and lipid synthesis in humans. We demonstrate, for the first time, that Cavin-2 deficiency causes insulin resistance and dyslipidemia with ectopic accumulation of fat in mice fed a high-fat diet. Genetic studies have shown the importance of PPARγ in glucose homeostasis in white adipocytes as well as in adipogenesis. Mice with activated PPARγ are protected from obesity-associated insulin resistance [43], whereas mice lacking PPARγ in the adipose tissue developed insulin resistance [44]. In humans, patients with a dominant-negative mutation in PPARγ have severe insulin resistance [45]. Thiazolidinedione (TZD), a high-affinity agonist for PPARγ, used as an anti-diabetic drug, improves glucose tolerance and promotes adipogenesis in adipocytes. Together with the results of in vitro studies, our in vivo results suggest that impaired glucose tolerance and lipid abnormalities caused by Cavin-2 deficiency are due to the suppression of IR/Akt/PPARγ signaling.

It was not evident that changes in IR expression or stability by Cavin-2 can be directly translated into changes in insulin signaling in mature adipocytes. To answer this question, we evaluated the expression of insulin receptors, and related proteins in eWAT in Cavin-2 KO mice fed a high-fat diet. The IRβ protein expression level and Akt phosphorylation in eWAT were significantly decreased in Cavin-2 KO mice compared to WT mice. Regazzetti et al. have reported that Cavin-2 silencing decreases IR phosphorylation in mature adipocytes, and Cavin-2 correlated negatively with HOMA-IR and glycated hemoglobin level [46]. These results, including ours, suggest that Cavin-2 in mature adipocytes affects insulin signaling, and Cavin-2 deficiency can have insulin resistance and risk developing diabetes-related complications.

Cavin-2-deficient mice showed enlarged adipocytes and had reduced number of adipocytes per unit area in WAT, similar to that seen in patients with metabolic syndrome. WAT in patients with metabolic syndrome shows hypertrophied adipocytes; the size and number of adipocytes in WAT from obese individuals correlate well with the risk of metabolic syndrome [47]. In contrast, WAT in healthy individuals contains a large number of relatively small adipocytes generated through adipogenesis. Our results suggest that Cavin-2 may play a significant role in the homeostasis of adipogenesis and lipid metabolism. Cavin-2 may reduce the risk of pathological obesity by promoting precise adipogenesis.

Some caveolae-related proteins are involved in lipodystrophy and lipid metabolism homeostasis. Defects in caveola-related proteins, such as CAV1 and Cavin-1, have been reported to impair adipogenesis. CAV1 mutations cause generalized or partial lipodystrophy with hypertriglyceridemia [48,49]. Human Cavin-1 mutations cause muscular dystrophy with generalized lipodystrophy [17]. Cavin-1 knockout mice have high levels of circulating triglycerides, significant adipose tissue loss, glucose intolerance, and hyperinsulinemia [18]. Although no disease caused by abnormalities in *Cavin*-2 has been reported to date, our findings suggest that loss-of-function mutants of Cavin-2 can cause lipodystrophy with glucose intolerance and dyslipidemia. Cavin-2 may also involve lipid metabolism homeostasis because the expression of Ucp-1, a marker of energy metabolism in lipids, decreased in Cavin-2 KO mice. Although not a Cavin mutation, LMNA mutations with the same lipodystrophy phenotype are associated with autophagy activation, hypertrophic adipocyte formation typical of white adipocytes, and brown fat dysregulation [50]. Although further studies using adipocyte-specific Cavin-2 KO mice are needed to answer the role of energy metabolism on Cavin-2, the same mechanism as LMNA mutation may be involved in Cavin-2 KO mice. We believe that Cavin-2 is a multifunctional scaffold protein on caveolae that not only cooperates with other caveolae-related proteins to regulate caveolae morphology and number but also regulates the stability and function of receptors involved in adipogenic differentiation and cell metabolism. Promoting adipogenesis via caveolar-related proteins might be one of the possible treatments for pathological obesity and lipodystrophy.

We propose a new function for Cavin-2 in adipogenesis. First, Cavin-2 promotes the stabilization of the insulin receptor and contributes to the efficient transduction of insulin receptor signals at the beginning of adipogenesis. Next, the Akt signal activated by the insulin receptor promotes the upregulation of PPARγ and C/EBPα and promotes adipogenesis while regulating the expression of various mRNAs involved in adipogenesis. The expression of Cavin-2 and insulin receptor is also downstream of the Akt signal and is stimulated. Thus, Cavin-2 may be involved in assisting in the formation of a positive feedback loop of committed adipogenesis.

In conclusion, we demonstrate that Cavin-2 is a crucial molecule for the stability and persistence of insulin/IR/Akt signaling for proper adipogenesis and lipid metabolism. Our findings highlight the pivotal role of Cavin-2 in adipogenesis and lipid metabolism, which may help develop novel therapies for pathological obesity and adipogenic disorders like lipodystrophy.

SOURCES OF FUNDING

This work was supported in part by the Japan Society for the Promotion of Science Grants-in-Aid for Scientific Research (JSPS KAKENHI) Grant Number JP18K07046.

AUTHOR CONTRIBUTIONS

Y.H. and T.O. wrote the manuscript and prepared figures. N.N. and S.M. took part in manuscript writing. Y.H. and T.O. conceived and designed the study. Y.H. and T.O. designed the experiments. Y.H. performed most of the experiments. T.O., N.N., M.N., A.S., Y.T., and S.T. contributed to in vitro and in vivo experiments. T.O. and S.M. participated in data interpretation.

ACKNOWLEDGMENTS

None.

CONFLICT OF INTEREST

The authors declare no conflict of interest.

APPENDIX A. SUPPLEMENTARY DATA

Supplementary data to this article can be found online at https://doi.org/10.1016/j.molmet.2021.101416.

REFERENCES

[1] Birsoy, K., Festuccia, W.T., Laplante, M., 2013. A comparative perspective on lipid storage in animals. Journal of Cell Science 126(Pt 7):1541–1552.

[2] Ghaben, A.L., Scherer, P.E., 2019. Adipogenesis and metabolic health. Nature Reviews Molecular Cell Biology 20(4):242–258.

[3] McLaughlin, T., Sherman, A., Tsao, P., Gonzalez, O., Yee, G., Lamendola, C., et al., 2007. Enhanced proportion of small adipose cells in insulin-resistant vs insulin-sensitive obese individuals implicates impaired adipogenesis. Diabetologia 50(8):1707–1715.

[4] Vishvanath, L., Gupta, R.K., 2019. Contribution of adipogenesis to healthy adipose tissue expansion in obesity. Journal of Clinical Investigation 129(10):4022–4031.

[5] Yang, J., Eliasson, B., Smith, U., Cushman, S.W., Sherman, A.S., 2012. The size of large adipose cells is a predictor of insulin resistance in first-degree relatives of type 2 diabetic patients. Obesity 20(5):932–938.

[6] Weisberg, S.P., McCann, D., Desai, M., Rosenbaum, M., Leibel, R.L., Ferrante Jr., A.W., 2003. Obesity is associated with macrophage accumulation in adipose tissue. Journal of Clinical Investigation 112(12):1796–1808.

[7] Rosen, E.D., Sarraf, P., Troy, A.E., Bradwin, G., Moore, K., Milstone, D.S., et al., 1999. PPAR gamma is required for the differentiation of adipose tissue in vivo and in vitro. Molecular Cell 4(4):611–617.

[8] Tontonoz, P., Hu, E., Spiegelman, B.M., 1994. Stimulation of adipogenesis in fibroblasts by PPAR gamma 2, a lipid-activated transcription factor. Cell 79(7):1147–1156.

[9] Foti, M., Porcheron, G., Fournier, M., Maeder, C., Carpentier, J.L., 2007. The neck of caveolae is a distinct plasma membrane subdomain that concentrates insulin receptors in 3T3-L1 adipocytes. Proceedings of the National Academy of Sciences of the United States of America 104(4):1242–1247.

[10] McMahon, K.A., Wu, Y., Gambin, Y., Sierecki, E., Tillu, V.A., Hall, T., et al., 2019. Identification of intracellular cavin target proteins reveals cavin-PP1alpha interactions regulate apoptosis. Nature Communications 10(1):3279.

[11] Parton, R.G., Simons, K., 2007. The multiple faces of caveolae. Nature Reviews Molecular Cell Biology 8(3):185–194.

[12] Cohen, A.W., Hnasko, R., Schubert, W., Lisanti, M.P., 2004. Role of caveolae and caveolins in health and disease. Physiological Reviews 84(4):1341–1379.

[13] Lamaze, C., Tardif, N., Dewulf, M., Vassilopoulos, S., Blouin, C.M., 2017. The caveolae dress code: structure and signaling. Current Opinion in Cell Biology 47:117–125.

[14] Nabi, I.R., 2009. Cavin fever: regulating caveolae. Nature Cell Biology 11(7):789–791.

[15] Kovtun, O., Tillu, V.A., Ariotti, N., Parton, R.G., Collins, B.M., 2015. Cavin family proteins and the assembly of caveolae. Journal of Cell Science 128(7):1269–1278.

[16] Ogata, T., Naito, D., Nakanishi, N., Hayashi, Y.K., Taniguchi, T., Miyagawa, K., et al., 2014. MURC/Cavin-4 facilitates recruitment of ERK to caveolae and concentric cardiac hypertrophy induced by α1-adrenergic receptors. Proceedings of the National Academy of Sciences of the United States of America 111(10):3811–3816.

[17] Hayashi, Y.K., Matsuda, C., Ogawa, M., Goto, K., Tominaga, K., Mitsuhashi, S., et al., 2009. Human PTRF mutations cause secondary deficiency of caveolins resulting in muscular dystrophy with generalized lipodystrophy. Journal of Clinical Investigation 119(9):2623–2633.

[18] Liu, L., Brown, D., McKee, M., Lebrasseur, N.K., Yang, D., Albrecht, K.H., et al., 2008. Deletion of Cavin/PTRF causes global loss of caveolae, dyslipidemia, and glucose intolerance. Cell Metabolism 8(4):310–317.

[19] Minetti, C., Sotgia, F., Bruno, C., Scartezzini, P., Broda, P., Bado, M., et al., 1998. Mutations in the caveolin-3 gene cause autosomal dominant limb-girdle muscular dystrophy. Nature Genetics 18(4):365–368.

[20] Park, P.J., Kim, S.T., 2020. Caveolae-associated protein 3 (Cavin-3) influences adipogenesis via TACE-mediated pref-1 shedding. International Journal of Molecular Sciences 21(14).

[21] Uhlén, M., Fagerberg, L., Hallström, B.M., Lindskog, C., Oksvold, P., Mardinoglu, A., et al., 2015. Proteomics. Tissue-based map of the human proteome. Science 347(6220):1260419.

[22] Bastiani, M., Liu, L., Hill, M.M., Jedrychowski, M.P., Nixon, S.J., Lo, H.P., et al., 2009. MURC/Cavin-4 and cavin family members form tissue-specific caveolar complexes. The Journal of Cell Biology 185(7):1259–1273.

[23] Hansen, C.G., Shvets, E., Howard, G., Riento, K., Nichols, B.J., 2013. Deletion of cavin genes reveals tissue-specific mechanisms for morphogenesis of endothelial caveolae. Nature Communications 4:1831.

[24] Hansson, B., Rippe, C., Kotowska, D., Wasserstrom, S., Säll, J., Göransson, O., et al., 2017. Rosiglitazone drives cavin-2/SDPR expression in adipocytes in a CEBPα-dependent manner. PLoS One 12(3):e0173412.

[25] Imoto-Tsubakimoto, H., Takahashi, T., Ueyama, T., Ogata, T., Adachi, A., Nakanishi, N., et al., 2013. Serglycin is a novel adipocytokine highly expressed in epicardial adipose tissue. Biochemical and Biophysical Research Communications 432(1):105–110.

[26] Ogata, T., Ueyama, T., Isodono, K., Tagawa, M., Takehara, N., Kawashima, T., et al., 2008. MURC, a muscle-restricted coiled-coil protein that modulates the Rho/ROCK pathway, induces cardiac dysfunction and conduction disturbance. Molecular and Cellular Biology 28(10):3424–3436.

[27] Nakanishi, N., Ogata, T., Naito, D., Miyagawa, K., Taniguchi, T., Hamaoka, T., et al., 2016. MURC deficiency in smooth muscle attenuates pulmonary hypertension. Nature Communications 7:12417.

[28] Naito, D., Ogata, T., Hamaoka, T., Nakanishi, N., Miyagawa, K., Maruyama, N., et al., 2015. The coiled-coil domain of MURC/cavin-4 is involved in membrane trafficking of caveolin-3 in cardiomyocytes. American Journal of Physiology - Heart and Circulatory Physiology 309(12):H2127–H2136.

[29] Folch, J., Lees, M., Sloane Stanley, G.H., 1957. A simple method for the isolation and purification of total lipides from animal tissues. Journal of Biological Chemistry 226(1):497–509.

[30] Nystrom, F.H., Chen, H., Cong, L.N., Li, Y., Quon, M.J., 1999. Caveolin-1 interacts with the insulin receptor and can differentially modulate insulin signaling in transfected Cos-7 cells and rat adipose cells. Molecular Endocrinology 13(12):2013–2024.

[31] Yamamoto, M., Toya, Y., Schwencke, C., Lisanti, M.P., Myers Jr., M.G., Ishikawa, Y., 1998. Caveolin is an activator of insulin receptor signaling. Journal of Biological Chemistry 273(41):26962–26968.

[32] Park, B.O., Ahrends, R., Teruel, M.N., 2012. Consecutive positive feedback loops create a bistable switch that controls preadipocyte-to-adipocyte conversion. Cell Reports 2(4):976–990.

[33] El-Jack, A.K., Hamm, J.K., Pilch, P.F., Farmer, S.R., 1999. Reconstitution of insulin-sensitive glucose transport in fibroblasts requires expression of both PPARgamma and C/EBPalpha. Journal of Biological Chemistry 274(12): 7946–7951.

[34] Rosen, E.D., Hsu, C.H., Wang, X., Sakai, S., Freeman, M.W., Gonzalez, F.J., et al., 2002. C/EBPalpha induces adipogenesis through PPARgamma: a unified pathway. Genes & Development 16(1):22–26.

[35] Wu, Z., Rosen, E.D., Brun, R., Hauser, S., Adelmant, G., Troy, A.E., et al., 1999. Cross-regulation of C/EBP alpha and PPAR gamma controls the transcriptional pathway of adipogenesis and insulin sensitivity. Molecular Cell 3(2):151–158.

[36] Hansen, C.G., Bright, N.A., Howard, G., Nichols, B.J., 2009. SDPR induces membrane curvature and functions in the formation of caveolae. Nature Cell Biology 11(7):807–814.

[37] Saltiel, A.R., Kahn, C.R., 2001. Insulin signalling and the regulation of glucose and lipid metabolism. Nature 414(6865):799–806.

[38] Zhang, H.H., Huang, J., Düvel, K., Boback, B., Wu, S., Squillace, R.M., et al., 2009. Insulin stimulates adipogenesis through the Akt-TSC2-mTORC1 pathway. PLoS One 4(7):e6189.

[39] Baudry, A., Yang, Z.Z., Hemmings, B.A., 2006. PKBalpha is required for adipose differentiation of mouse embryonic fibroblasts. Journal of Cell Science 119(Pt 5):889–897.

[40] Xu, J., Liao, K., 2004. Protein kinase B/AKT 1 plays a pivotal role in insulin-like growth factor-1 receptor signaling induced 3T3-L1 adipocyte differentiation. Journal of Biological Chemistry 279(34):35914–35922.

[41] Ross, S.E., Erickson, R.L., Hemati, N., MacDougald, O.A., 1999. Glycogen synthase kinase 3 is an insulin-regulated C/EBPalpha kinase. Molecular and Cellular Biology 19(12):8433–8441.

[42] Liu, L., Pilch, P.F., 2016. PTRF/Cavin-1 promotes efficient ribosomal RNA transcription in response to metabolic challenges. Elife 5.

[43] Rangwala, S.M., Rhoades, B., Shapiro, J.S., Rich, A.S., Kim, J.K., Shulman, G.I., et al., 2003. Genetic modulation of PPARgamma phosphorylation regulates insulin sensitivity. Developmental Cell 5(4):657–663.

[44] He, W., Barak, Y., Hevener, A., Olson, P., Liao, D., Le, J., et al., 2003. Adipose-specific peroxisome proliferator-activated receptor gamma knockout causes insulin resistance in fat and liver but not in muscle. Proceedings of the National Academy of Sciences of the United States of America 100(26):15712–15717.

[45] Barroso, I., Gurnell, M., Crowley, V.E., Agostini, M., Schwabe, J.W., Soos, M.A., et al., 1999. Dominant negative mutations in human PPARgamma associated with severe insulin resistance, diabetes mellitus and hypertension. Nature 402(6764):880–883.

[46] Regazzetti, C., Dumas, K., Lacas-Gervais, S., Pastor, F., Peraldi, P., Bonnafous, S., et al., 2015. Hypoxia inhibits Cavin-1 and Cavin-2 expression and down-regulates caveolae in adipocytes. Endocrinology 156(3):789–801.

[47] Laforest, S., Labrecque, J., Michaud, A., Cianflone, K., Tchernof, A., 2015. Adipocyte size as a determinant of metabolic disease and adipose tissue dysfunction. Critical Reviews in Clinical Laboratory Sciences 52(6):301–313.

[48] Kim, C.A., Delépine, M., Boutet, E., El Mourabit, H., Le Lay, S., Meier, M., et al., 2008. Association of a homozygous nonsense caveolin-1 mutation with Berardinelli-Seip congenital lipodystrophy. Journal of Clinical Endocrinology & Metabolism 93(4):1129–1134.

[49] Cao, H., Alston, L., Ruschman, J., Hegele, R.A., 2008. Heterozygous CAV1 frameshift mutations (MIM 601047) in patients with atypical partial lipodystrophy and hypertriglyceridemia. Lipids in Health and Disease 7:3.

[50] Pellegrini, C., Columbaro, M., Schena, E., Prencipe, S., Andrenacci, D., Iozzo, P., et al., 2019. Altered adipocyte differentiation and unbalanced autophagy in type 2 Familial Partial Lipodystrophy: an in vitro and in vivo study of adipose tissue browning. Experimental & Molecular Medicine 51(8):1–17.

